THE JOURNAL OF BIOLOGICAL CHEMISTRY VOL. 287, NO. 7, pp. 4662–4670, February 10, 2012

Determination of the Proton Environment of High Stability Menasemiquinone Intermediate in *Escherichia coli* Nitrate Reductase A by Pulsed EPR*[S]

Received for publication, November 18, 2011, and in revised form, December 21, 2011 Published, JBC Papers in Press, December 21, 2011, DOI 10.1074/jbc.M111.325100

Stéphane Grimaldi[‡1], Rodrigo Arias-Cartin[§2], Pascal Lanciano[‡3], Sevdalina Lyubenova[¶4], Rodolphe Szenes[‡], Burkhard Endeward[¶], Thomas F. Prisner[¶], Bruno Guigliarelli[‡], and Axel Magalon[§]

From the [‡]Unité de Bioénergétique et Ingénierie des Protéines (UPR9036) and [§]Laboratoire de Chimie Bactérienne (UPR9043), Institut de Microbiologie de la Méditerranée, CNRS and Aix-Marseille University, 13009 Marseille, France and the [¶]Institut für Physikalische und Theoretische Chemie, University of Frankfurt, 60438 Frankfurt, Germany

Background: *Escherichia coli* nitrate reductase A highly stabilizes a semiquinone catalytic intermediate.
Results: Three proton hyperfine couplings to this radical with atypical characteristics are characterized.
Conclusion: Semiquinone binding is strongly asymmetric and occurs via a single short in-plane H-bond.
Significance: Learning how the protein environment tunes the semiquinone properties is crucial for understanding the quinol utilization mechanism by energy-transducing enzymes.

Escherichia coli **nitrate reductase A (NarGHI) is a membrane-bound enzyme that couples quinol oxidation at a periplasmically oriented Q-site (Q_D) to proton release into the periplasm during anaerobic respiration. To elucidate the molecular mechanism underlying such a coupling, endogenous menasemiquinone-8 intermediates stabilized at the Q_D site (MSQ_D) of NarGHI have been studied by high-resolution pulsed EPR methods in combination with $^1H_2O/^2H_2O$ exchange experiments. One of the two non-exchangeable proton hyperfine couplings resolved in hyperfine sublevel correlation (HYSCORE) spectra of the radical displays characteristics typical from quinone methyl protons. However, its unusually small isotropic value reflects a singularly low spin density on the quinone carbon α carrying the methyl group, which is ascribed to a strong asymmetry of the MSQ_D binding mode and consistent with single-sided hydrogen bonding to the quinone oxygen O1. Furthermore, a single exchangeable proton hyperfine coupling is resolved, both by comparing the HYSCORE spectra of the radical in ^1H_2O and ^2H_2O samples and by selective detection of the exchanged deuterons using Q-band ^2H Mims electron nuclear double resonance (ENDOR) spectroscopy. Spectral analysis reveals its peculiar characteristics, *i.e.* a large anisotropic hyperfine coupling together with an almost zero isotropic contribution. It is assigned to a proton involved in a short ~1.6 Å in-plane hydrogen bond between the quinone O1 oxygen and the Nδ of the His-66 residue, an axial ligand of the distal heme b_D. Structural and mechanistic implications of these results for the electron-coupled proton translocation mechanism at the Q_D site are discussed, in light of the unusually high thermodynamic stability of MSQ_D.**

Quinones are small lipophilic organic molecules found in energy-transducing membranes of all living organisms except methanogens (1). Due to their ability to transfer up to two electrons and two protons, they are widely used in photosynthetic and respiratory electron transfer chains. Quinones can freely diffuse in the hydrophobic core of lipid membranes. They can therefore bind into specific quinone-reactive sites (Q-sites)[5] of membrane proteins in which they function as two-electron and proton carriers and are responsible for exchange of reducing equivalents between different electron transport complexes. In this case, the quinones leave the protein after completion of the redox cycle. Typical examples are the Q_B site of bacterial reaction center (RC) or photosystem II and the Q-sites (Q_o and Q_i) of bc_1 complex. In contrast, non-dissociable quinones can be tightly bound at specific quinone-reactive sites of proteins in which they can be involved in electron transfer processes as prosthetic groups. Well known representatives of this type include quinones in the Q_A site in RCs of purple bacteria and in photosystem II or the A_1 sites in photosystem I (2, 3).

* This work was supported by the CNRS, the Agence Nationale de la Recherche, and Aix-Marseille Université. This work was also supported by Research Infrastructures Activity in the 6th Framework Program of the European Community (Contract RII3-026145, EU-NMR) for financial support (to S. G.), as well as the European Cooperation in Science and Technology Action (COST P15) "Advanced Paramagnetic Resonance Methods in Molecular Biophysics" for Short-Term Scientific Mission funding (to S. G.).
[S] This article contains supplemental Figs. S1 and S2 and Tables S1 and S2.
[1] To whom correspondence may be addressed: Unité de Bioénergétique et Ingénierie des Protéines (BIP – CNRS UPR9036), Institut de Microbiologie de la Méditerranée, CNRS and Aix-Marseille Université, 31, chemin Joseph Aiguier 13402 Marseille cedex 20, France. Tel.: 33-491-164-557; Fax: 33-491-164-097; E-mail: grimaldi@ifr88.cnrs-mrs.fr.
[2] Present address: Dept. of Molecular, Cellular and Developmental Biology, Yale University, New Haven, CT 06520.
[3] Present address: Dept. of Biology, University of Pennsylvania, Philadelphia, PA 19104.
[4] Present address: EPR Division, Bruker BioSpin GmbH, 76287 Rheinstetten, Germany.

[5] The abbreviations used are: Q-site, quinone-reactive site; Q, quinone; SQ, semiquinone; QH_2, quinol; ENDOR, electron nuclear double resonance; ESE, electron spin echo; ESEEM, electron spin echo envelope modulation; HYSCORE, hyperfine sublevel correlation; IMV, inner membrane vesicle; MSQ_D, menasemiquinone stabilized at the Q_D site of NarGHI; USQ_D, ubisemiquinone stabilized at the Q_D site of NarGHI; NarGHI, membrane-bound form of the native enzyme complex; RC, photosynthetic reaction center; mT, milliteslas.

The different redox states of quinones may also adopt different conformations in the quinone-binding pockets, as evidenced for ubiquinone and ubisemiquinone at the Q_B site of bacterial RC (4). The functional diversity of Q-sites arises from a particular tuning of the protein environment. Despite the fact that high-resolution structural data are available for several Q-sites, how protein-cofactor interactions relate to and control the functional properties of the bound quinone is largely unknown. In particular, understanding the molecular mechanism underlying the coupling between electron transfer and proton translocation that occurs at dissociable Q-sites requires obtaining structural information on all three forms, quinone (Q), semiquinone (SQ), and quinol (QH_2). For this purpose, high-resolution EPR methods such as ENDOR (electron nuclear double resonance) and ESEEM (electron spin echo envelope modulation) spectroscopies were proven to be valuable by giving detailed structural information on protein-bound semiquinone intermediates, provided that this paramagnetic state can be trapped for spectroscopic studies.

Escherichia coli nitrate reductase A (NarGHI) is a membrane-bound heterotrimeric enzyme induced by anaerobiosis and the presence of nitrate. Involved in the nitrate respiratory pathway, a major alternative to the bacterial oxidative phosphorylation, it couples the oxidation of menaquinols or ubiquinols at a periplasmically oriented Q-site (named Q_D) to the cytoplasmic reduction of nitrate. Thus, both substrate turnovers contribute to the generation of a proton motive force across the cytoplasmic membrane. NarGHI contains eight redox-active metal centers (5–9): a molybdenum cofactor and an Fe_4S_4 cluster (FS0) in the nitrate-reducing subunit NarG; one Fe_3S_4 cluster (FS4) and three Fe_4S_4 clusters (FS1–3) in the electron transfer subunit NarH; and two low spin hemes b in the membrane-anchor subunit NarI, termed b_D and b_P to indicate their distal and proximal position to the catalytic site. Importantly, NarI stabilizes an EPR-detectable semiquinone intermediate of both natural substrates at its quinol oxidation site Q_D close to heme b_D (10–12). Remarkably, the resulting menasemiquinone species herein referred to as MSQ_D has the largest thermodynamic stability measured so far in respiratory complexes stabilizing semiquinone intermediates. These peculiar properties render NarGHI ideally suited for investigating the molecular factors responsible for the reactivity of respiratory enzymes toward quinols.

Although no high-resolution structural data revealing the binding mode of the natural quinol/quinone substrate are available, we recently utilized high-resolution EPR techniques on endogenous MSQ_D and ubisemiquinone radical (USQ_D) stabilized in NarGHI-enriched inner membrane vesicles (IMVs) of *E. coli* to explore their environment using the unpaired electron as a probe. The use of ESEEM and HYSCORE (hyperfine sublevel correlation) spectroscopies on either the wild-type enzyme or the enzyme uniformly enriched with ^{15}N nuclei provided direct evidence for nitrogen ligation to MSQ_D and USQ_D. On the basis of the direct determination of the quadrupolar parameters of the corresponding interacting ^{14}N by S-band (~3 GHz) HYSCORE experiments, we assigned the latter to an N_δ imidazole nitrogen and proposed it to arise from the heme b_D axial ligand His-66 (13). The non-zero isotropic hyperfine coupling of this nitrogen suggests that the interaction occurs via a hydrogen bond, allowing electron spin density to be transferred from the radical to the interacting nucleus. Interestingly, these experiments did not support a direct H-bond between MSQ_D (or USQ_D) and Lys-86, a residue in the Q_D site that was previously shown to be essential for quinol oxidation and menasemiquinone detection (11, 14). Indeed, no evidence for the transfer of a measurable spin density on any other nuclei than that mentioned above was found. Thus, we tentatively proposed that a water-mediated interaction is formed between MSQ_D (or USQ_D) and Lys-86, consistent with the latter being involved in reactivity toward quinols (13). Moreover, we have recently shown that a cardiolipin molecule specifically bound to the complex is necessary for quinol substrate fixation at the Q_D site, probably through the action of one of its acyl chains located in the vicinity of His-66 (15). Clearly, additional information is required to improve our understanding of the semiquinone binding mode in the Q_D site and of its functional tuning by the protein environment.

In this work, high-resolution EPR techniques have been used to map the environment and the binding mode of MSQ_D via the detection of proton hyperfine couplings to the radical. Using a combination of X-band (~9 GHz) ESEEM/HYSCORE and Q-band (~34 GHz) Mims ENDOR experiments on MSQ_D prepared in either a protonated or a deuterated solvent, one exchangeable and two non-exchangeable protons magnetically coupled to the radical were detected. Their detailed characterization allows their assignment to specific protons in the vicinity of the radical. Implications of these results for deciphering the semiquinone binding mode and the catalytic mechanism at the Q_D site are discussed.

EXPERIMENTAL PROCEDURES

Sample Preparation—NarGHI was expressed in an *E. coli* nitrate reductase-deficient strain LCB3063 (RK4353, Δ*napA-B, narG*::*ery,* Δ*narZ*::Ω, Spc^R) (16) using pVA700 plasmid (Amp^R) (6), which encodes for the *narGHJI* operon under control of the tac promoter. Cells were grown in Terrific Broth under semi-anaerobic conditions at 37 °C as described in Ref. 11 with ampicillin (100 μg ml^{-1}) and spectinomycin (50 μg ml^{-1}) included in the growth medium.

Purified *E. coli* NarGHI-enriched IMVs were used for this study, allowing us to maintain an unmodified lipid environment and to study the interaction of NarGHI with its endogenous menaquinol substrate. For this purpose, purified *E. coli* NarGHI-enriched IMVs were isolated by differential centrifugation and sucrose gradient step as described in Ref. 11 using a buffer containing 100 mM MOPS and 5 mM EDTA at pH 7.5. Deuterium-exchanged samples were prepared using the same membrane extraction protocol with a buffer containing ^2H_2O (99.9% atom ^2H) instead of ^1H_2O. The functionality of NarGHI in our samples was confirmed spectrophotometrically by measuring the quinol:nitrate oxidoreductase activity. Stabilization of the semiquinone at the Q_D site was achieved through redox titrations under the same conditions as those used in our previous works (10, 11, 13). Redox potentials are given in the text with respect to the standard hydrogen electrode. The semiquinone concentration in our samples estimated from the double

integration of their corresponding EPR spectra and by comparison with a standard (1 mM $CuSO_4$) was estimated in the range of 10–12 μM.

Pulsed EPR/ENDOR Experiments—X-band (~9 GHz) and Q-band (~34 GHz) pulsed EPR/ENDOR experiments were performed using a Bruker EleXsys E580-Q spectrometer equipped with an Oxford Instruments CF 935 cryostat. Spectra were measured at 90 K to avoid contamination from fast relaxing metal centers such as FeS centers in NarGHI (13). For the two-pulse experiments ($\pi/2$-τ-π), the echo intensity was measured as a function of magnetic field at fixed time interval τ between the two microwave pulses for field sweep ESE or as a function of τ at a fixed magnetic field value for two-pulse ESEEM.

Two-pulse and four-pulse ($\pi/2$-τ-$\pi/2$-T/2-π-T/2-$\pi/2$) ESEEM and HYSCORE ($\pi/2$-τ-$\pi/2$-t_1-π-t_2-$\pi/2$) experiments were performed at a magnetic field corresponding to the maximum intensity of the MSQ_D two-pulse field sweep ESE spectrum where all orientations of the semiquinone with respect to the external magnetic field contribute, giving rise to powder ESEEM/HYSCORE spectra (see the supplemental material). Spectra were processed using the Bruker Xepr software. Relaxation decays were subtracted (fitting by polynomial functions) followed by zero-filling and tapering with a Hamming window, before Fourier transformation, which finally gives the spectrum in frequency domain. All spectra are shown in absolute value mode. HYSCORE spectra are presented as contour plots.

Q-band pulsed ^{2}H ENDOR spectra were obtained using the Mims ($\pi/2$-τ-$\pi/2$-t-$\pi/2$-τ-echo) sequence (17). A radio frequency π pulse was applied during the time interval t. The radio frequency power was delivered by a 2-kilowatt Dressler solid state radio frequency amplifier. It was optimized for radio frequency π pulse lengths of 40 μs for deuterium Mims ENDOR experiments. Pulsed ENDOR spectra were recorded at a magnetic field corresponding to the $g_\perp$ position of the nearly axial Q-band EPR signal of MSQ_D (10). Pulsed EPR/ENDOR spectra were simulated in the MATLAB environment using the Easyspin software package (release 3.1.0) (18).

Hyperfine and Quadrupole Interactions—A hyperfine coupling between an S = ½ radical and a nucleus with nuclear spin value I consists in general of (i) the isotropic contribution $A_{iso} = 2\mu_0 g_e g_n \beta_e \beta_n |\psi_0(0)|^2/3h$, where $|\psi_0(0)|^2$ is the electron spin density at the nucleus, g_e and g_n are electron and nuclear g-factors, respectively, β_e and β_n are Bohr and nuclear magnetons, respectively, h is Planck's constant, and (ii) the anisotropic contribution described by the traceless dipolar coupling tensor $\tilde{T}$. In most cases, $\tilde{T}$ can be assumed to be axial, with principal values (−T, −T, 2T).

The hyperfine couplings of different isotopes of the same element are proportional to a very good approximation to the corresponding g_n values. In this study, the direct and simultaneous determination of A_{iso} and T of the protons interacting with MSQ_D were derived from the analysis of HYSCORE cross-peak contours as detailed in the supplemental material (19).

A ^{2}H nucleus has a quadrupole moment that interacts with the electric field gradient at the nucleus. The components of the electric field gradient tensor are defined in its principal axis system and ordered according to $|q_{ZZ}| \geq |q_{YY}| \geq |q_{XX}|$. This traceless tensor can then be fully described by only two parameters: (i) the ^{2}H nuclear quadrupole coupling constant $\kappa = |e^2 q_{ZZ} Q/h|$, where e is the charge of electron, Q is the ^{2}H nuclear electric quadrupole moment; and (ii) the asymmetry parameter $\eta = |q_{YY} - q_{XX}/q_{ZZ}|$. κ is a measure of the strength of the interaction between the nuclear quadrupole moment and the electric field gradient at the ^{2}H nucleus site due to anisotropic charge distribution around the nucleus, whereas η is a measure of the deviation of this distribution from axial symmetry. Thus, the electric field gradient is related to the specific binding geometry. Its components can, therefore, be used to obtain detailed information on hydrogen bonds (20–26). In this study the parameters κ and η of the ^{2}H interacting with MSQ_D were estimated by simulation of the Q-band ^{2}H Mims ENDOR spectrum.

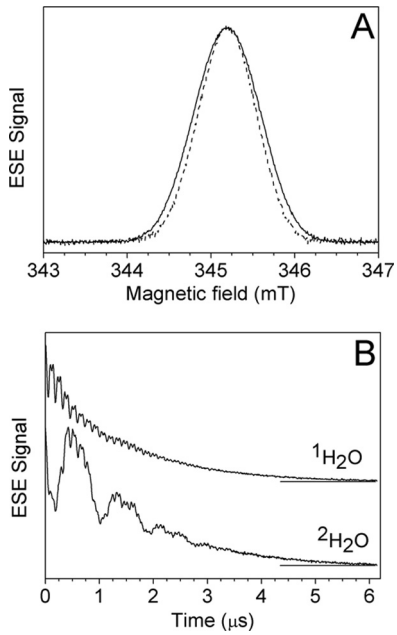

FIGURE 1. **Two-pulse experiments of MSQ_D.** *A*, field sweep ESE spectra in redox-poised samples prepared in ^1H_2O (−107 mV, *solid line*) and ^2H_2O (−106 mV, *dotted lines*). *B*, ESEEM patterns of the corresponding samples in ^1H_2O (*top*) and ^2H_2O (*bottom*). For the sample in ^1H_2O, the microwave frequency was 9.6912 GHz, and the magnetic field was 345.2 mT. For the sample in ^2H_2O, these were 9.6899 GHz and 345.3 mT, respectively.

RESULTS

X-band Pulsed EPR (Field Sweep, Two-pulse ESEEM)—X-band field sweep ESE spectra of NarGHI-enriched IMVs were recorded at 90 K in samples redox-poised at ~−100 mV prepared in either ^1H_2O or ^2H_2O. They show a single line from the MSQ stabilized at the Q_D site of NarGHI with g ~2.0045 and the width ~0.8 mT in ^1H_2O (13). Replacement of ^1H_2O by ^2H_2O decreases the line width by less than 0.1 mT (Fig. 1*A*). The weakness of this effect is due to the primary contribution to the line shape of the g-tensor anisotropy, which was previously resolved using numerical simulation of the MSQ_D Q-band EPR spectrum (10). The two-pulse spin echo decay of the radical measured in ^1H_2O at 90 K is depicted in Fig. 1*B*. It mainly shows the modulation associated with weakly coupled protons in the immediate environment, with Zeeman frequencies $\nu_I(^1H)$

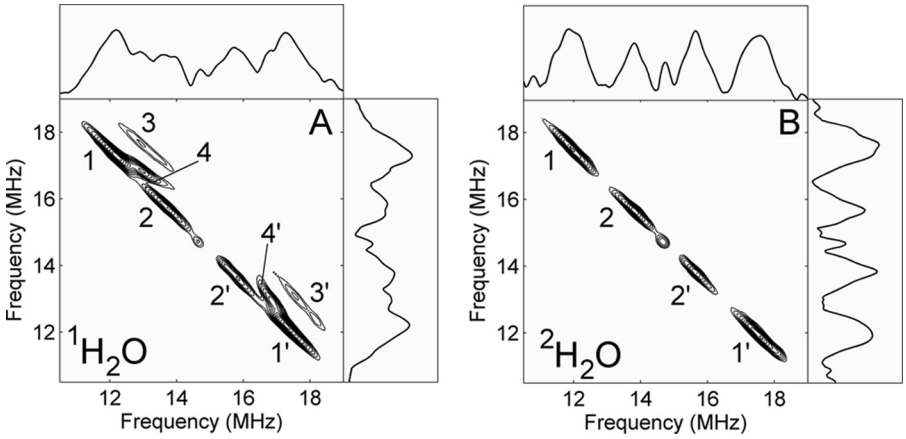

FIGURE 2. **Proton part of HYSCORE spectra of MSQ_D in ^1H_2O (*A*) or in ^2H_2O (*B*) with time $\tau = 204$ ns.** The microwave frequency was 9.6944 GHz (*A*) and 9.6934 GHz (*B*), and the magnetic field was 345.2 mT. For both spectra, the durations of the $\pi/2$ and π pulses were 12 and 24 ns, respectively, with equal amplitude. 256 points were recorded in each dimension. t_1 and t_2 were incremented in steps of 16 ns from their initial value.

~14.7 MHz. A characteristic deep additional modulation of the echo intensity appears in the sample prepared in ^2H_2O (Fig. 1*B*). Fourier transformation of this echo envelope reveals that the major contribution to the deep variations occurs at the frequency ~2.3 MHz, corresponding to the Zeeman frequency of deuterium (not shown). These results give a first indication of solvent accessibility and $^1H/^2H$ exchange around MSQ_D. To increase spectral resolution and thus provide more detailed information about the proton environment of MSQ_D, HYSCORE experiments were carried out and are shown below.

X-band ^1H HYSCORE—The low frequency parts of the X-band HYSCORE spectra of MSQ_D were previously shown and analyzed in detail. They revealed cross-peaks arising from a single ^{14}N hyperfine coupling assigned to the heme b_D ligand His-66 residue (12, 13). In addition to these ^{14}N signals, several cross-features from protons symmetrically positioned with respect to the ^1H Zeeman frequency ($\nu_I(^1H)$ ~14.7 MHz) are clearly resolved in the 10–20-MHz frequency range in the (+,+) quadrant of these spectra (Fig. 2*A*). This indicates that several protons are magnetically coupled to the radical. The appearance of these correlations in the (+,+) quadrant indicates that the corresponding hyperfine couplings for a given proton satisfy the relationships $|T+2A_{iso}| \ll 4\nu_I(^1H)$ (27). To further analyze the spectrum and discriminate between exchangeable and non-exchangeable features, HYSCORE experiments were also performed under the same conditions in the sample prepared in ^2H_2O. Fig. 2 shows the proton region of the corresponding HYSCORE spectra recorded with $\tau = 204$ ns in ^1H_2O (Fig. 2*A*) or ^2H_2O (Fig. 2*B*). In addition to the diagonal peak at $\nu_I(^1H)$ ~14.7 MHz, four pairs of cross-features located symmetrically relative to the diagonal are well resolved in the spectrum shown in Fig. 2*A*. They are designated 1, 1′, 2, 2′, 3, 3′, 4, and 4′. The ridges 2-2′ exhibit the smallest resolved hyperfine splitting, of the order of ~2 MHz, whereas the largest one is observed for cross-peaks 1-1′. Cross-ridges 3-3′ possess the most extended anisotropic contour, with the largest deviation from the diagonal, whereas cross-peaks 4-4′ deviate significantly from the normal to the diagonal. These two features indicate a significant anisotropic hyperfine component. Contours 1-1′ and 2-2′ are approximately normal to the diagonal, suggesting a smaller anisotropy. Cross-peaks 1 and 4 partially overlap.

TABLE 1

Hyperfine tensors derived from contour line shape analysis of HYSCORE spectra

$A_\perp$ is the component of the hyperfine tensor where the direction of magnetic field is perpendicular to the symmetry axis of the axially symmetric hyperfine tensor, and $A_\parallel$, the component where the direction of magnetic field is parallel to it (see the supplemental data). $A_{iso} = 1/3(2A_\perp + A_\parallel)$. The preferred sets are indicated in bold (see "Discussion").

	(A_{iso}, T) MHz	$\lvert A_\perp\rvert = \lvert A_{iso}-T\rvert$	$\lvert A_\parallel\rvert = \lvert A_{iso}+2T\rvert$	$\lvert(A_\parallel-A_\perp)/A_{iso}\rvert$	Assignment
H1a	∓ 6.78, ±1.25	8.03	4.28	0.55	methyl protons
H1b	**±5.53, ±1.25**	**4.28**	**8.03**	**0.68**	
H2a	∓ 2.14, ±1.18	3.32	0.22	1.3	β-methylene proton
H2b	**±0.96, ±1.18**	**0.22**	**3.32**	**3.2**	
H3a	∓ 5.79, ±5.73	11.52	5.67	1.01	H-bond proton
H3b	**±0.06, ±5.73**	**5.67**	**11.52**	**97.5**	

Cross-peaks 3-3′ and 4-4′ completely disappear in the proton HYSCORE spectrum measured in ^2H_2O, demonstrating that they are produced by at least one exchangeable proton (Fig. 2*B*). In contrast, cross-peaks 1-1′ and 2-2′ still appear in the spectrum measured in ^2H_2O, showing that they arise from non-exchangeable (*i.e.* covalently bound) protons.

Quantitative analysis of the cross-peak contour line shapes indicates that cross-peaks 3, 3′, 4, and 4′ are produced by a single exchangeable proton (supplemental Fig. S2 and supplemental Table S1). Hence, HYSCORE signals derive from three protons coupled to MSQ_D: H1 (1-1′), H2 (2-2′), and H3 (3-3′-4-4′). Among them, H3 is exchangeable. The isotropic (A_{iso}) and anisotropic (T) components of the three ^1H hyperfine tensors are given in Table 1. The magnitude of the hyperfine couplings deduced from the analysis of HYSCORE spectra are consistent with our previous preliminary observations of ^1H continuous wave ENDOR resonances with corresponding estimated hyperfine couplings A_1 ~5.7 MHz (H3) and A_2 ~3.3 MHz (H2) (10, 11).

X-band ^1H Four-pulse ESEEM—Additional information about the interacting protons was obtained from one-dimensional four-pulse ESEEM spectra, which are particularly useful for the observation of proton sum combination lines with improved resolution (27, 28). The four-pulse ESEEM spectrum

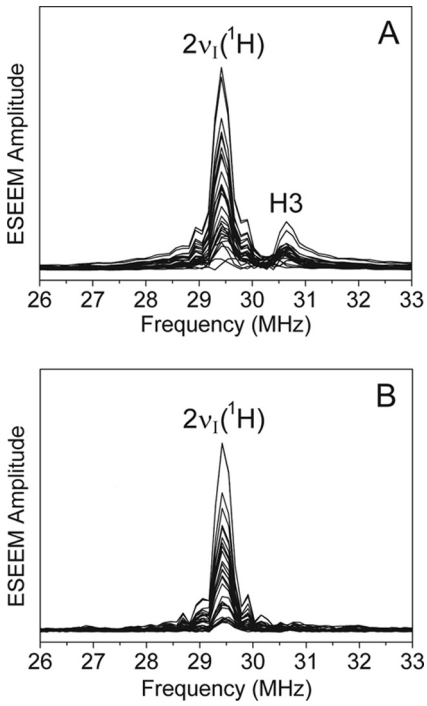

FIGURE 3. **Stacked presentations of the two-dimensional set of the four-pulse ESEEM spectra of MSQ_D in ^1H_2O (*A*) and ^2H_2O (*B*).** The spectra show modulus Fourier transforms along the time T/2 axis (1024 points with a 4 ns step) at 30 different times τ. The initial τ is 96 ns and was increased by 8 ns in successive traces. The microwave frequency was 9.6912 GHz (*A*) and 9.6898 GHz, and the magnetic field was 345.2 mT (*A*) and 345.4 mT (*B*).

of MSQ_D in ^1H_2O buffer contains two well resolved lines in the region of the proton around $2\nu_I(^1H)$ as shown in Fig. 3*A*. The most intense line appears exactly at the $2\nu_I(^1H)$ frequency and represents the contribution of weakly coupled protons from the protein environment. In addition, the spectrum exhibits a peak of lower intensity shifted from $2\nu_I(^1H)$ to higher frequencies by ~1.2 MHz. This shifted peak completely disappears in the spectra of the sample prepared in ^2H_2O (Fig. 3*B*). This indicates that the line shifted from $2\nu_I(^1H)$ arises from an exchangeable proton. The shift observed in the four-pulse ESEEM is well described by

$$\Delta = 9T^2/16\nu_I(^1H) \qquad \text{(Eq. 1)}$$

from which the anisotropic component T of the hyperfine coupling can be estimated (see supplemental material). The shift of ~1.2 MHz corresponds to T = 5.7 MHz, which is in very good agreement with the corresponding value determined for H3 from the analysis of the HYSCORE spectra. The expected shifts from H1 and H2 (0.06 and 0.05 MHz, respectively) are too small to be resolved in a four-pulse ESEEM spectrum (supplemental Table S2). The proton sum combination peak therefore confirms the assignment made in the HYSCORE spectra for the exchangeable proton and the hyperfine coupling determined from these spectra.

Q-band ^2H Mims ENDOR—Further details concerning exchangeable protons coupled to MSQ_D were obtained through the use of pulsed ^2H ENDOR spectroscopy. Fig. 4 shows the Q-band ^2H Mims ENDOR spectrum of MSQ_D in NarGHI-enriched IMVs prepared in ^2H_2O. It has been

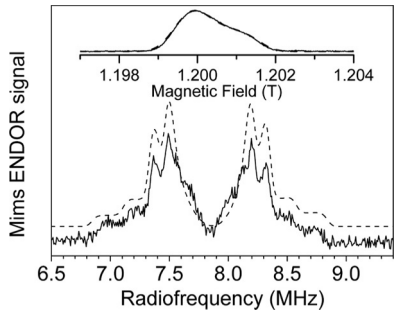

FIGURE 4. **Q-band ^2H Mims ENDOR spectrum of MSQ_D in ^2H_2O.** Experimental conditions were as follows: microwave pulse length, 24 ns; microwave frequency, 33.684926 GHz; magnetic field value, 1.1999 T; measurement time, 20 h. The simulated spectrum (*dotted lines*) was generated from the following parameters: a single hyperfine tensor with components (A_{iso} = 0.06/6.5, ~0.009 MHz, T = 5.73/6.5, ~0.88 MHz) and with nuclear quadrupole coupling parameters (κ = 0.18 MHz, η = 0.2), with g-, A-, and Q- collinear to each other. The Q-band field-swept ESE spectrum of MSQ_D is shown on *top*. Its simulation, shown as *dotted lines*, has been performed using the g-tensor principal values given under "Results," an isotropic convolutional Gaussian line width with full width at half-maximum of 0.76 mT. Experimental conditions were as follows: microwave pulse lengths, 24 and 48 ns for $\pi/2$ and π pulses, respectively; microwave frequency, 33.68504 GHz.

recorded at a magnetic field value corresponding to the maximum intensity of the nearly axially symmetric Q-band EPR spectrum of MSQ_D with g-tensor principal values g_x = 2.0061, g_y = 2.0051, g_z = 2.0023 ± 0.0001 (Fig. 4, *top*) (10). The ENDOR spectrum exhibits two pairs of well resolved intense lines located symmetrically with respect to the ^2H nuclear Larmor frequency ($\nu_I(^2H)$ ~7.84 MHz) and subject to the nuclear quadrupole interaction. The splitting of their center away from the Larmor frequency (~0.8 MHz) is determined by the hyperfine coupling constant, and the splitting within the pair (~0.13 MHz) is given by the quadrupole interaction. The same holds for the two pairs of less intense lines resolved in the spectrum shown in Fig. 4, separated by ~1.5 MHz and split each by ~0.26 MHz. The hyperfine coupling values of ~0.8 and ~1.5 MHz are first estimates of the $A_\perp$ and $A_\parallel$ components of an almost purely dipolar hyperfine tensor. They are very close to those found for H3 and scaled to the ^2H nucleus, *i.e.* $A_\perp$ = 0.87 and $A_\parallel$ = 1.77 MHz. Similarly, a nuclear quadrupole coupling constant $\kappa \sim \frac{4}{3} \times 0.13$ ~0.173 MHz can be estimated from the 0.13-MHz splitting of the two most intense doublets. A numerical simulation of the spectrum is shown in Fig. 4. It was obtained using the proton hyperfine coupling values of H3 deduced from the analysis of the HYSCORE spectra and rescaled by the factor $g_n(^1H)/g_n(^2H)$ ~6.5. This best simulation was obtained assuming that the g-, A-, and Q-tensors are collinear, with quadrupole parameters κ = (0.176 ± 0.004) MHz and η = 0.20 ± 0.05. Finally, this procedure allowed us to select unambiguously the right set ($|A_{iso}|$, $|T|$) for H3 from the two alternatives (Table 1). Overall, the data show that a single exchangeable proton is coupled to the radical, in agreement with the analysis above.

DISCUSSION

Single Exchangeable Proton Coupling with Peculiar Hyperfine Coupling Characteristics—Our data clearly show the presence of a single exchangeable proton in the vicinity of MSQ_D characterized by $|A_{iso}|$ = 0.06 MHz and $|T|$ = 5.73 MHz. Such hyperfine coupling constants are in the range of those measured for

exchangeable protons coupled to protein-bound semiquinones and assigned to protons hydrogen-bonded to the quinone carbonyl oxygens. Typical examples include exchangeable proton couplings to the menasemiquinone stabilized at the Q_H site of the aa_3 menaquinol oxidase from *Bacillus subtilis* ($|T| = 5.6$ MHz and $|A_{iso}| = 5.4$ MHz) or to the photoaccumulated phyllosemiquinone $A_1^{\bullet -}$ in *Thermococcus elongatus* photosystem I ($|T| \sim 3.7$ MHz and $|A_{iso}| \sim 0.1$ MHz) (29, 30). Thus, we assign H3 to a proton involved in H-bonding to one of the MSQ_D carbonyl oxygens. However, the hyperfine coupling tensor to H3 has atypical properties as it combines both an almost zero isotropic hyperfine coupling constant A_{iso} and a large anisotropic part T. The magnitude of the H-bond tensor is determined by the geometry of the H-bond. A small A_{iso} is expected when the H-bond lies in the molecular plane due to the small overlap between the hydrogen 1*s* orbital and the oxygen 2*pz* orbital forming part of the semiquinone singly occupied molecular orbital. Almost purely anisotropic hyperfine tensors have thus been observed for in-plane hydrogen-bonded protons to unsubstituted quinones measured in alcoholic solvent, whereas the corresponding |T| values do not exceed 3 MHz (23, 24, 31, 32). The T value measured for H3 is one of the largest measured so far for a proton hydrogen-bonded to a semiquinone. According to density functional theory calculations, the large T value of H3 is predicted to account for a short hydrogen-bond length, typically in the range of 1.3–1.4 Å (22). In this case, Sinnecker *et al.* (21, 22, 24) have shown that the point dipole model does not work due to the increased covalent character of the H-bond that is not covered in the point dipole approximation. A more reliable alternative approach is to evaluate H-bond distances from the nuclear quadrupole coupling constant of ^2H. As empirically proposed by Soda and Chiba (25) and Hunt and Mackay (26), it has been shown that the nuclear quadrupole coupling constant of ^2H nuclei H-bonded to semiquinones follows a $r^{-3}(O–^2H)$ dependence of the form

$$\kappa = a - \frac{b}{r^3(O–^2H)}[kHz] \qquad \text{(Eq. 2)}$$

where a and b are empirical parameters (22). Using $a = 319$ kHz and $b = 607$ kHz Å^3 (20) and the value of $\kappa = 176 \pm 4$ kHz deduced from our work, we obtain from Equation 2 a bond length of $r(O–^2H) = 1.62 \pm 0.02$ Å. This value is in the range of short hydrogen bonds for biological systems. For instance, it is similar to that formed from the carbonyl oxygen O4 of the ubisemiquinone $Q_A^{\bullet -}$ in the RC from *Rhodobacter sphaeroides* R-26 to the imidazole nitrogen Nδ of His M219 ($r(O–^2H) = 1.60 \pm 0.04$ Å) (20).

Assignment of Non-exchangeable Proton Couplings—In addition to H3, two non-exchangeable proton couplings H1 and H2 are clearly resolved in the HYSCORE spectra of MSQ_D measured in ^2H_2O. For their assignment, we rely on previous experimental and theoretical studies on phylloquinone (also called vitamin K_1) and menaquinone (vitamin K_2) radicals examined in liquid and solid organic solvents or in proteins (23, 29, 30, 33–37). Indeed, these quinones share the same naphthoquinone ring structure methylated at the second position but differ in their aliphatic side chain attached at the 3-position (see supplemental Fig. S1). It has been shown both experimentally and theoretically that the aliphatic side chain properties have only a weak influence on the proton hyperfine coupling tensors measured in organic solvents (23, 33, 34, 38, 39). From these previous studies, it is evident that the non-exchangeable proton couplings from H1 and H2 > 2 MHz originate from the ring methyl protons, from the β-methylene isoprenyl protons, or from α-protons directly attached to the quinone ring. Due to rapid rotation of the methyl group even at low temperature, methyl protons of vitamin K molecules have equal hyperfine tensors and give prominent ENDOR/ESEEM signals. They are characterized by an almost axial hyperfine tensor, a predominant isotropic hyperfine coupling value in the range of 6.8–12.3 MHz, and a characteristic relative hyperfine anisotropy $(A_{\|} - A_{\perp})/A_{iso}$ in the range of 0.26–0.45 with $A_{\|} > A_{\perp} > 0$. The latter value increases up to 0.76 for the methyl protons of the asymmetrically bound ubisemiquinone $Q_A^{\bullet -}$ in the RC from *R. sphaeroides* (2). Based on these results, we assign H1 to the methyl protons of MSQ_D, with $A_{iso} = +5.53$ MHz and $T = +1.25$ MHz leading to a $(A_{\|} - A_{\perp})/A_{iso}$ value of ~0.68 (Fig. 5).

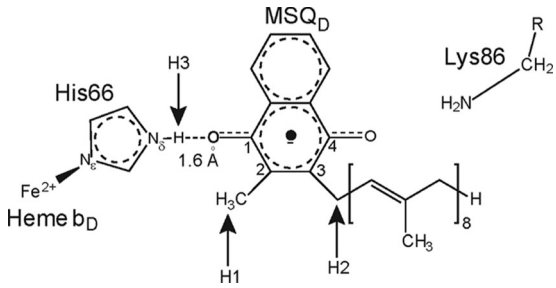

FIGURE 5. **Working model of MSQ_D binding mode in *E. coli* NarGHI based on our spectroscopic work.** Strongly asymmetric binding of MSQ_D occurs via a short in-plane H-bond to the N_δ of His-66, whereas Lys-86 does not appear to be a direct H-bond donor to the radical in the semiquinone state (13). The MSQ_D O4 oxygen is deprotonated. The protons H1, H2, and H3 discussed under "Results" are indicated by *arrows*. r = NHCCO$(CH_2)_3$.

Hyperfine data for β-methylene protons and ring α protons in semiquinones are less abundant. Unlike the methyl protons, the methylene protons are not expected to rotate freely (40). They are also characterized by a nearly axial hyperfine tensor with $A_{\|} > A_{\perp} > 0$ (40, 41). In contrast, a high degree of anisotropy is expected for a ring α proton hyperfine tensor due to the short distance of the proton and the spin density (30, 40). Because of the axial symmetry of its hyperfine coupling tensor, we tentatively assign H2 to one of the β-methylene isoprenyl protons with $A_{iso} = +0.96$ MHz and $T = +1.18$ MHz (Fig. 5). Overall, the ^1H hyperfine coupling constants determined in this work are consistent with those estimated from our previous continuous wave X-band ^1H ENDOR studies of MSQ_D (10, 11).

Strongly Asymmetric Spin Distribution in MSQ_D—The ^1H hyperfine coupling constants are an excellent probe of the asymmetry of the spin density distribution in the quinone. In particular, the predominant isotropic component, A_{iso}, of hyperfine coupling to the methyl protons is directly proportional to the unpaired spin density in the π orbital on the adjacent α-carbon (ρ_C), as described by the McConnell relation, $A_{iso} = \rho_C B_2/2$, where B_2 has been taken in the range from 120 to 212 MHz (42). The corresponding value for the methyl protons of MSQ_D ($A_{iso} = 5.53$ MHz) is the smallest one ever reported

for these protons for vitamin K molecules bound to proteins or in protic solvents (23, 29, 30, 33, 34, 36, 38, 39). In particular, the spin density on the Cα at the 2-position, which is sensed by the methyl protons, is reduced by ~30% in MSQ_D as compared with the symmetrically hydrogen bonded MSQ-4 prepared in 2-propanol (39). This decrease can be explained by a strong asymmetry of hydrogen bonding to the carbonyl oxygens of MSQ_D in NarGHI, which leads to a redistribution of both the spin density and charges within the quinone ring (2, 43, 44). Indeed, a stronger hydrogen bond to the carbonyl oxygen O1, as compared with oxygen O4, is expected to lead to an increase of spin density on carbon 3 but a decrease of the spin density on carbon 2 as observed here for MSQ_D. A similar but less pronounced spin density shift has been proposed for the menasemiquinone-9 in the Q_A site of the RC from *Rhodopseudomonas viridis* for which the methyl protons isotropic hyperfine coupling constant is about 6.8 MHz (39). In contrast, the large isotropic constants for methyl protons of the MSQ-7 in the aa_3 menaquinol oxidase from *B. subtilis* (A_{iso} ~11.0 MHz) (29) or of the radical anion of phylloquinone in the A_1 site of photosystem I from *Thermosynechococcus elongatus* (A_{iso} = 9.8 MHz) (30) suggest that a stronger hydrogen bond to oxygen O4 is formed as compared with oxygen O1, a strongly asymmetric binding mode reverse to that observed in NarGHI.

Model for MSQ_D Binding to NarGHI and Mechanistic Implications—Altogether, the data inferred from the present work allow us to refine the MSQ_D binding model previously proposed (13). We conclude that the asymmetrical spin density distribution in MSQ_D is primarily due to the strong hydrogen bond formed to the O1 oxygen of MSQ_D involving the exchangeable H3 proton coupling (Fig. 5). Hence, the latter appears mostly responsible for the transfer of spin density from the radical to the interacting nitrogen nucleus that was deduced from the measurement of a small ^{14}N isotropic hyperfine coupling of A_{iso} ~0.8 MHz to MSQ_D using HYSCORE spectroscopy. Based on the measurement of its nuclear quadrupole parameters by S-band HYSCORE spectroscopy (κ = 0.49, η = 0.50), this nucleus was assigned to the N_δ imidazole nitrogen from the heme b_D axial ligand His-66 (13). In addition, this model is consistent with the relatively small η value found for this imidazole nitrogen that is close to that predicted by density functional theory calculations on imidazoles forming a strong in-plane hydrogen bond to one of the benzosemiquinone oxygen atoms (45). Finally, the presence of the positive charges on the nearby heme Fe^{2+} ion may also contribute to the observed asymmetrical spin distribution in MSQ_D.

Interestingly, a single strong and highly ordered H-bond to MSQ_D was detected in the present work by using both ^1H HYSCORE and ^2H Q-band ENDOR spectroscopies. In the most recent studies of protein-bound semiquinones, the radicals appear to be coupled to at least two exchangeable protons assigned to those involved in H-bonds (20, 29, 46–49). One-sided H-bond was resolved only for the photoaccumulated phyllosemiquinone $A_1^{\bullet-}$ in photosystem I (30, 50). Based on their experimental and theoretical results, Niklas *et al.* (30) have shown that the single detected short ~1.64 Å H-bond can fully account for the observed asymmetry in the spin density distribution of the SQ in the A_1 site. Remarkably, both the H-bond length and the ~30% variation of the spin density on the Cα at the 2-position of the phyllosemiquinone in the A_1 site with respect to the symmetrically hydrogen-bonded radical are comparable with the corresponding values measured for MSQ_D. Thus, our results indicate that MSQ_D most likely binds to the protein via a one-sided H-bond.

Consequently, our present work indicates that the O4 carbonyl oxygen of MSQ_D is not protonated in this intermediate state, showing that at least one proton has to be released to the periplasm consecutively to the first electron transfer step to heme b_D. This step likely involves Lys-86, a residue that is located at the protein surface, at the entrance of the Q_D cavity, and that is required for correct binding of quinol analogues and for semiquinone detection at the Q_D site of NarGHI (11, 13, 14). Thus, we speculate that Lys-86 could be a direct hydrogen bond donor to the quinol molecule, facilitating proton abstraction at the quinol O4 oxygen and, concomitantly, the first electron transfer step. This would be accompanied by a movement of Lys-86 away from the substrate, leading to an asymmetric binding mode of the semiquinone intermediate and allowing for proton release toward the periplasm (Fig. 5). Whether quinol deprotonation at the O1 oxygen is coupled to the first or the second electron transfer step remains unclear. Additional studies aimed at measuring the pH dependence of the redox reactions occurring at the Q_D site will be useful to further understanding how quinol deprotonation and electron transfer are synchronized at the Q_D site. Such studies are currently being performed in our laboratories.

Role of Protein Environment in Quinol Utilization and Semiquinone Stabilization—The high stabilization of MSQ_D in NarGHI is directly related to the redox potentials of the redox transitions MQH_2/MSQ ($E_{m,7.5}$ = −150 mV) and MSQ/MQ ($E_{m,7.5}$ = −40 mV), which are both thermodynamically favorable for electron transfer to the b_D heme (10). We questioned whether the unusually high stabilization of the semiquinone state at the NarGHI Q_D site can be related to the strongly asymmetric binding mode of MSQ_D mainly due to the short in-plane H-bond formed to the radical. Remarkably, the two other protein-bound semiquinones with redox properties most strongly affected by the protein environment as compared with the corresponding species in alcoholic solvents are the very low potential (E_m ~−750 mV) phyllosemiquinone anion $A_1^{\bullet-}$ in photosystem I and the high affinity ubisemiquinone at the Q_H site of cytochrome bo_3, which has a high stability, albeit 10 times smaller than that measured for MSQ_D. In both cases, the semiquinones interact with the protein environment in a very asymmetric manner (46, 51–53). This contrasts to the much lower stability of the more symmetrically bound semiquinones at the Q_B site of photosynthetic bacterial RC (48, 54) or at the Q_i site in *R. sphaeroides* bc_1 complex (47, 55). In addition, the strong H-bond to MSQ_D is expected to withdraw electron density and stabilize the semiquinone form, thereby raising the redox potential of the second oxidation step from semiquinone to quinone, as experimentally measured. Consequently, we hypothesize that the atypical binding mode of MSQ_D could strongly contribute to its unusual redox properties. In addition, other effects such as the electrostatic environment of the nearby protein should also be taken into account. Evaluating

their respective contribution to the MSQ_D redox properties requires further work. Finally, the functional implications of this high stabilization remain to be established.

It has been shown both experimentally and theoretically that the presence of bulky substituents on the quinone ring force hydrogen-bond formation out-of-plane, thereby increasing simultaneously the isotropic and anisotropic coupling of the hydrogen-bonded protons (32, 56). Remarkably, measurement of a small A_{iso} and a simultaneous large T value for the proton hydrogen-bonded to MSQ_D indicates that the protein environment around the radical strongly constrains the geometry of the hydrogen bond by maintaining a short in-plane H-bond to the radical, thus leading to the observed peculiar hyperfine coupling characteristics. We have recently shown that an endogenous USQ_D can also be stabilized at the NarGHI Q_D site (12). It binds to the protein via an H-bond to the same nitrogen as menasemiquinone does, *i.e.* most likely His-66 N_δ. The similar ^{14}N HYSCORE pattern observed for both radicals suggests that the H-bond involved in binding USQ_D has similar characteristics to that detected in the present study. This provides further support for its involvement in ubisemiquinone stabilization at the Q_D site. Finally, our work indicates that the protein environment counteracts the effect of the presence of bulky substituents to impose an atypical binding mode. Further work is in progress in our laboratories to evaluate the importance of the quinone substituents to accommodate and utilize various substrates at this Q-site and to stabilize semiquinone intermediates.

Concluding Remarks—From the experiments reported in this work, we conclude that MSQ_D is involved in a single strong in-plane and highly ordered H-bond with a solvent exchangeable proton. This strongly asymmetric binding causes a shift of the electron spin density over the quinone ring consistent with the formation of a strong hydrogen bond to the quinone carbonyl oxygen O1. This peculiar binding mode could strongly contribute to the unusual redox properties of MSQ_D.

Acknowledgments—We thank Guillaume Gerbaud and Emilien Etienne for maintenance of the Aix-Marseille EPR facility and Patrick Bertrand and Frédéric Biaso for helpful discussions.

REFERENCES

1. Nicholls, D. G., and Ferguson, S. J. (2002) *Bioenergetics*, Third Ed., Academic Press, London
2. Lubitz, W., and Feher, G. (1999) The primary and secondary acceptors in bacterial photosynthesis III. Characterization of the quinone radicals $Q_A^{\bullet -}$ and $Q_B^{\bullet -}$ by EPR and ENDOR. *Appl. Magn. Reson.* **17,** 1–48
3. Srinivasan, N., and Golbeck, J. H. (2009) Protein-cofactor interactions in bioenergetic complexes: the role of the A_{1A} and A_{1B} phylloquinones in photosystem I. *Biochim. Biophys. Acta* **1787,** 1057–1088
4. Stowell, M. H., McPhillips, T. M., Rees, D. C., Soltis, S. M., Abresch, E., and Feher, G. (1997) Light-induced structural changes in photosynthetic reaction center: implications for mechanism of electron-proton transfer. *Science* **276,** 812–816
5. Lanciano, P., Savoyant, A., Grimaldi, S., Magalon, A., Guigliarelli, B., and Bertrand, P. (2007) New method for the spin quantitation of $[4Fe\text{-}4S]^+$ clusters with $S = ½$: application to the FS0 center of the NarGHI nitrate reductase from *Escherichia coli*. *J. Phys. Chem. B* **111,** 13632–13637
6. Guigliarelli, B., Magalon, A., Asso, M., Bertrand, P., Frixon, C., Giordano, G., and Blasco, F. (1996) Complete coordination of the four Fe-S centers of the β subunit from *Escherichia coli* nitrate reductase: physiological, biochemical, and EPR characterization of site-directed mutants lacking the highest or lowest potential [4Fe-4S] clusters. *Biochemistry* **35,** 4828–4836
7. Blasco, F., Guigliarelli, B., Magalon, A., Asso, M., Giordano, G., and Rothery, R. A. (2001) The coordination and function of the redox centers of the membrane-bound nitrate reductases. *Cell Mol. Life Sci.* **58,** 179–193
8. Rothery, R. A., Blasco, F., Magalon, A., and Weiner, J. H. (2001) The diheme cytochrome *b* subunit (NarI) of *Escherichia coli* nitrate reductase A (NarGHI): structure, function, and interaction with quinols. *J. Mol. Microbiol. Biotechnol.* **3,** 273–283
9. Bertero, M. G., Rothery, R. A., Palak, M., Hou, C., Lim, D., Blasco, F., Weiner, J. H., and Strynadka, N. C. (2003) Insights into the respiratory electron transfer pathway from the structure of nitrate reductase A. *Nat. Struct. Biol.* **10,** 681–687
10. Grimaldi, S., Lanciano, P., Bertrand, P., Blasco, F., and Guigliarelli, B. (2005) Evidence for an EPR-detectable semiquinone intermediate stabilized in the membrane-bound subunit NarI of nitrate reductase A (NarGHI) from *Escherichia coli*. *Biochemistry* **44,** 1300–1308
11. Lanciano, P., Magalon, A., Bertrand, P., Guigliarelli, B., and Grimaldi, S. (2007) High stability semiquinone intermediate in nitrate reductase A (NarGHI) from *Escherichia coli* is located in a quinol oxidation site close to heme b_D. *Biochemistry* **46,** 5323–5329
12. Arias-Cartin, R., Lyubenova, S., Ceccaldi, P., Prisner, T., Magalon, A., Guigliarelli, B., and Grimaldi, S. (2010) HYSCORE evidence that endogenous mena- and ubisemiquinone bind at the same Q site (Q_D) of *Escherichia coli* nitrate reductase A. *J. Am. Chem. Soc.* **132,** 5942–5943
13. Grimaldi, S., Arias-Cartin, R., Lanciano, P., Lyubenova, S., Endeward, B., Prisner, T. F., Magalon, A., and Guigliarelli, B. (2010) Direct evidence for nitrogen ligation to the high stability semiquinone intermediate in *Escherichia coli* nitrate reductase A. *J. Biol. Chem.* **285,** 179–187
14. Bertero, M. G., Rothery, R. A., Boroumand, N., Palak, M., Blasco, F., Ginet, N., Weiner, J. H., and Strynadka, N. C. (2005) Structural and biochemical characterization of a quinol-binding site of *Escherichia coli* nitrate reductase A. *J. Biol. Chem.* **280,** 14836–14843
15. Arias-Cartin, R., Grimaldi, S., Pommier, J., Lanciano, P., Schaefer, C., Arnoux, P., Giordano, G., Guigliarelli, B., and Magalon, A. (2011) Cardiolipin-based respiratory complex activation in bacteria. *Proc. Natl. Acad. Sci. U.S.A.* **108,** 7781–7786
16. Potter, L. C., Millington, P., Griffiths, L., Thomas, G. H., and Cole, J. A. (1999) Competition between *Escherichia coli* strains expressing either a periplasmic or a membrane-bound nitrate reductase: does Nap confer a selective advantage during nitrate-limited growth? *Biochem. J.* **344,** 77–84
17. Mims, W. B. (1965) Pulsed ENDOR experiments. *Proc. R. Soc. Lond. Ser. A* **283,** 452–457
18. Stoll, S., and Schweiger, A. (2006) EasySpin, a comprehensive software package for spectral simulation and analysis in EPR. *J. Magn. Reson.* **178,** 42–55
19. Dikanov, S. A., and Bowman, M. K. (1995) Cross-peak lineshape of two-dimensional ESEEM spectra in disordered $S = ½$, $I = ½$ spin systems. *J. Magn. Reson.* **116,** 125–128
20. Flores, M., Isaacson, R., Abresch, E., Calvo, R., Lubitz, W., and Feher, G. (2007) Protein-cofactor interactions in bacterial reaction centers from *Rhodobacter sphaeroides* R-26: II: geometry of the hydrogen bonds to the primary quinone formula by ^1H and ^2H ENDOR spectroscopy. *Biophys. J.* **92,** 671–682
21. Sinnecker, S., Flores, M., and Lubitz, W. (2006) Protein-cofactor interactions in bacterial reaction centers from *Rhodobacter sphaeroides* R-26: effect of hydrogen bonding on the electronic and geometric structure of the primary quinone. A density functional theory study. *Phys. Chem. Chem. Phys.* **8,** 5659–5670
22. Sinnecker, S., Reijerse, E., Neese, F., and Lubitz, W. (2004) Hydrogen bond geometries from electron paramagnetic resonance and electron-nuclear double resonance parameters: density functional study of quinone radical anion-solvent interactions. *J. Am. Chem. Soc.* **126,** 3280–3290
23. Epel, B., Niklas, J., Sinnecker, S., Zimmermann, H., and Lubitz, W. (2006) Phylloquinone and related radical anions studied by pulse electron nuclear double resonance spectroscopy at 34 GHz and density functional theory. *J. Phys. Chem. B* **110,** 11549–11560

24. Flores, M., Isaacson, R. A., Calvo, R., Feher, G., and Lubitz, W. (2003) Probing hydrogen bonding to quinone anion radicals by ^{1}H and ^{2}H ENDOR Spectroscopy at 35 GHz. *Chem. Phys.* **294,** 401–413
25. Soda, G., and Chiba, T. (1969) Deuteron magnetic resonance study of cupric sulfate pentahydrate. *J. Chem. Phys.* **50,** 439–455
26. Hunt, M. J., and Mackay, A. L. (1974) Deuterium and nitrogen pure quadrupole resonance in deuterated amino acids. *J. Magn. Reson.* **15,** 402–414
27. Schweiger, A., and Jeschke, G. (2001) *Principles of Pulse Electron Paramagnetic Resonance*, Oxford University Press, New York
28. Reijerse, E. J., and Dikanov, S. A. (1991) Electron spin echo envelope modulation spectroscopy on orientationally disordered systems: Line shape singularities in S = ½, I = ½ spin systems. *J. Chem. Phys.* **95,** 836–845
29. Yi, S. M., Narasimhulu, K. V., Samoilova, R. I., Gennis, R. B., and Dikanov, S. A. (2010) Characterization of the semiquinone radical stabilized by the cytochrome aa_3-600 menaquinol oxidase of *Bacillus subtilis*. *J. Biol. Chem.* **285,** 18241–18251
30. Niklas, J., Epel, B., Antonkine, M. L., Sinnecker, S., Pandelia, M. E., and Lubitz, W. (2009) Electronic structure of the quinone radical anion $A_1^{\bullet-}$ of photosystem I investigated by advanced pulse EPR and ENDOR techniques. *J. Phys. Chem. B* **113,** 10367–10379
31. O'Malley, P. J., and Babcock, G. T. (1986) Powder ENDOR spectra of p-Benzoquinone anion radical: Principal hyperfine tensor components for ring protons and hydrogen-bonded protons. *J. Am. Chem. Soc.* **108,** 3995–4001
32. MacMillan, F., Lendzian, F., and Lubitz, W. (1995) EPR and ENDOR characterization of semiquinone anion radicals related to photosynthesis. *Magn. Reson. Chem.* **33,** S81–S93
33. Das, M. R., Connor, H. D., Leniart, D. S., and Freed, J. H. (1970) An electron nuclear double resonance and electron spin resonance study of semiquinones related to vitamins K and E. *J. Am. Chem. Soc.* **92,** 2258–2268
34. Teutloff, C., Bittl, R., and Lubitz, W. (2004) Pulse ENDOR studies on the radical pair P_{700}^{+} $A_1^{\bullet-}$ and the photoaccumulated quinone acceptor $A_1^{\bullet-}$ of photosystem I. *Appl. Magn. Reson.* **26,** 5–21
35. O'Malley, P. J. (1999) Density functional calculated spin densities and hyperfine couplings for hydrogen-bonded 1,4-naphthosemiquinone and phyllosemiquinone anion radicals: a model for the A_1 free radical formed in photosystem I *Biochim. Biophys. Acta* **1411,** 101–113
36. Hastings, S. F., Heathcote, P., Ingledew, W. J., and Rigby, S. E. (2000) ENDOR spectroscopic studies of stable semiquinone radicals bound to the *Escherichia coli* cytochrome bo_3 quinol oxidase. *Eur. J. Biochem.* **267,** 5638–5645
37. Rigby, S. E., Evans, M. C., and Heathcote, P. (2001) Electron nuclear double resonance (ENDOR) spectroscopy of radicals in photosystem I and related type 1 photosynthetic reaction centers. *Biochim. Biophys. Acta* **1507,** 247–259
38. Rigby, S. E., Evans, M. C., and Heathcote, P. (1996) ENDOR and special triple resonance spectroscopy of $A_1^{\bullet-}$ of photosystem 1. *Biochemistry* **35,** 6651–6656
39. Gardiner, A. T., Zech, S. G., MacMillan, F., Käss, H., Bittl, R., Schlodder, E., Lendzian, F., and Lubitz, W. (1999) Electron paramagnetic resonance studies of zinc-substituted reaction centers from *Rhodopseudomonas viridis*. *Biochemistry* **38,** 11773–11787
40. Zheng, M., and Dismukes, G. C. (1996) The conformation of the isoprenyl chain relative to the semiquinone head in the primary electron acceptor (Q_A) of higher plant PSII (plastosemiquinone) differs from that in bacterial reaction centers (ubisemiquinone or menasemiquinone) by ~90 degrees. *Biochemistry* **35,** 8955–8963
41. Kevan, L., and Kispert, L. D. (1976) *Electron Spin Double Resonance Spectroscopy*, John Wiley & Sons, Inc., New York
42. McConnell, H. M. (1956) Indirect hyperfine interactions in the paramagnetic resonance spectra of aromatic free radicals. *J. Chem. Phys.* **24,** 764–766
43. Lubitz, W., Abresch, E. C., Debus, R. J., Isaacson, R. A., Okamura, M. Y., and Feher, G. (1985) Electron nuclear double resonance of semiquinones in reaction centers of *Rhodopseudomonas sphaeroides*. *Biochim. Biophys. Acta* **808,** 464–469
44. Feher, G., Isaacson, R. A., Okamura, M. Y., and Lubitz, W. (1985) in *Antennas and Reaction Centers of Photosynthetic Bacteria* (Michel-Beyerle, M. E., ed) Vol. 42, pp. 174–189, Springer-Verlag, Berlin
45. Fritscher, J. (2004) Influence of hydrogen bond geometry on quadrupole coupling parameters: a theoretical study of imidazole–water and imidazole–semiquinone complexes. *Phys. Chem. Chem. Phys.* **6,** 4950–4956
46. Yap, L. L., Samoilova, R. I., Gennis, R. B., and Dikanov, S. A. (2006) Characterization of the exchangeable protons in the immediate vicinity of the semiquinone radical at the Q_H site of the cytochrome bo_3 from *Escherichia coli*. *J. Biol. Chem.* **281,** 16879–16887
47. Dikanov, S. A., Samoilova, R. I., Kolling, D. R., Holland, J. T., and Crofts, A. R. (2004) Hydrogen bonds involved in binding the Q_i site semiquinone in the bc_1 complex, identified through deuterium exchange using pulsed EPR. *J. Biol. Chem.* **279,** 15814–15823
48. Martin, E., Samoilova, R. I., Narasimhulu, K. V., Lin, T. J., O'Malley, P. J., Wraight, C. A., and Dikanov, S. A. (2011) Hydrogen bonding and spin density distribution in the Q_B semiquinone of bacterial reaction centers and comparison with the Q_A site. *J. Am. Chem. Soc.* **133,** 5525–5537
49. Chatterjee, R., Milikisiyants, S., Coates, C. S., and Lakshmi, K. V. (2011) High-resolution two-dimensional ^{1}H and ^{14}N hyperfine sublevel correlation spectroscopy of the primary quinone of photosystem II. *Biochemistry* **50,** 491–501
50. Srinivasan, N., Chatterjee, R., Milikisiyants, S., Golbeck, J. H., and Lakshmi, K. V. (2011) Effect of hydrogen bond strength on the redox properties of phylloquinones: a two-dimensional hyperfine sublevel correlation spectroscopy study of photosystem I. *Biochemistry* **50,** 3495–3501
51. Grimaldi, S., Ostermann, T., Weiden, N., Mogi, T., Miyoshi, H., Ludwig, B., Michel, H., Prisner, T. F., and MacMillan, F. (2003) Asymmetric binding of the high-affinity $Q_H^{\bullet-}$ ubisemiquinone in quinol oxidase (bo_3) from *Escherichia coli* studied by multifrequency electron paramagnetic resonance spectroscopy. *Biochemistry* **42,** 5632–5639
52. Kacprzak, S., Kaupp, M., and MacMillan, F. (2006) Protein-cofactor interactions and EPR parameters for the Q_H quinone-binding site of quinol oxidase: a density functional study. *J. Am. Chem. Soc.* **128,** 5659–5671
53. MacMillan, F., Kacprzak, S., Hellwig, P., Grimaldi, S., Michel, H., and Kaupp, M. (2011) Elucidating mechanisms in heme copper oxidases: the high-affinity Q_H-binding site in quinol oxidase as studied by DONUT-HYSCORE spectroscopy and density functional theory. *Faraday Discuss.* **148,** 315–344
54. Rutherford, A. W., and Evans, M. C. (1980) Direct measurement of the redox potential of the primary and secondary quinone electron acceptors in *Rhodopseudomonas sphaeroides* (wild-type) by EPR spectrometry. *FEBS Lett.* **110,** 257–261
55. Robertson, D. E., Prince, R. C., Bowyer, J. R., Matsuura, K., Dutton, P. L., and Ohnishi, T. (1984) Thermodynamic properties of the semiquinone and its binding site in the ubiquinol-cytochrome *c* (c_2) oxidoreductase of respiratory and photosynthetic systems. *J. Biol. Chem.* **259,** 1758–1763
56. O'Malley, P. J. (1998) A density functional study of the effect of orientation of hydrogen bond donation on the hyperfine couplings of benzosemiquinones: relevance to semiquinone-protein hydrogen bonding interactions *in vivo*. *Chem. Phys. Lett.* **291,** 367–374